Michigan Technological University

Michigan Technological University
Digital Commons @ Michigan Tech

Department of Physics Publications | Department of Physics

2-1-2014

# On-Chip Multi 4-Port Optical Circulators

Ramy El-Ganainy
*Michigan Technological University*

Miguel Levy
*Michigan Technological University*

Follow this and additional works at: https://digitalcommons.mtu.edu/physics-fp

 Part of the Atomic, Molecular and Optical Physics Commons, and the Optics Commons

## Recommended Citation

El-Ganainy, R., & Levy, M. (2014). On-Chip Multi 4-Port Optical Circulators. *IEEE Photonics Journal, 6(1).*
http://digitalcommons.mtu.edu/physics-fp/2/

Follow this and additional works at: https://digitalcommons.mtu.edu/physics-fp

 Part of the Atomic, Molecular and Optical Physics Commons, and the Optics Commons

IEEE Photonics Journal
An IEEE Photonics Society Publication

Open Access

# On-Chip Multi 4-Port Optical Circulators

Volume 6, Number 1, February 2014

**Ramy El-Ganainy**
**Miguel Levy**

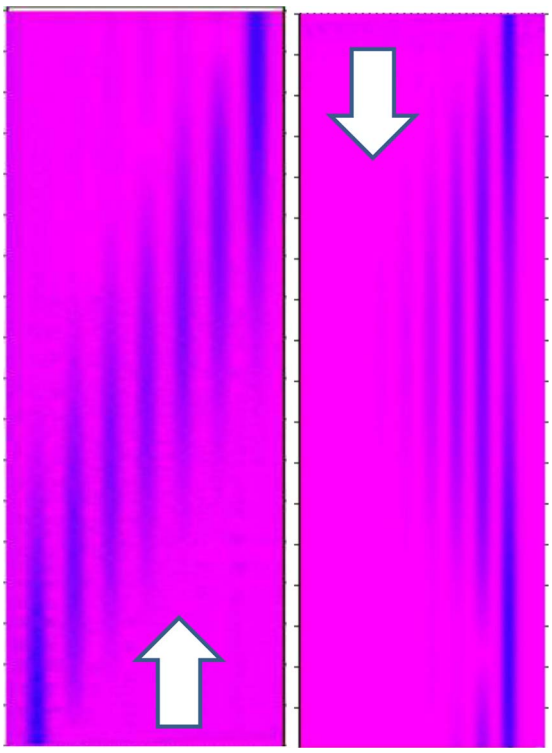

DOI: 10.1109/JPHOT.2013.2294693
1943-0655 © 2013 IEEE

IEEE photonics SOCIETY

IEEE

# On-Chip Multi 4-Port Optical Circulators

**Ramy El-Ganainy and Miguel Levy**

Department of Physics, Michigan Technological University, Houghton, MI 49931 USA

*DOI: 10.1109/JPHOT.2013.2294693*
*1943-0655 © 2013 IEEE. Translations and content mining are permitted for academic research only. Personal use is also permitted, but republication/redistribution requires IEEE permission. See http://www.ieee.org/publications_standards/publications/rights/index.html for more information.*

Manuscript received October 8, 2013; revised December 5, 2013; accepted December 6, 2013. Date of publication December 12, 2013; date of current version January 15, 2014. The work of M. Levy was supported by the Air Force Research Laboratory through the Advanced Materials, Manufacturing, and Testing Information Analysis Center under Alion Science and Technology Contract FA4600-06-D-0003 DO#0048. Corresponding author: M. Levy (e-mail: mlevy@mtu.edu).

**Abstract:** We present a new geometry for on-chip optical circulators based on waveguide arrays. The optical array is engineered to mimic the Fock space representation of a noninteracting two-site Bose–Hubbard Hamiltonian. By introducing a carefully tailored magneto-optic nonreciprocity to these structures, the array operates in the perfect transfer and surface Bloch oscillation modes in the forward and backward propagation directions, respectively. We show that an array made of $(2N + 1)$ waveguide channels can function as $N$ 4-port optical circulators with very large isolation ratios and low forward losses. Numerical analysis using beam propagation method indicates a large bandwidth of operation.

**Index Terms:** Magnetic devices, isolators, optical devices, optical arrays, optical waveguides, ferrimagnetic films.

## 1. Introduction

Photonic devices are important key players in present day technology. They find applications in different and diverse engineering fields ranging from communication networks, optical interconnects, bio-imaging to medical surgery [1]. In the last decades, significant research activity has been conducted to miniaturize different optical components. While these efforts have been largely successful, a certain class of nonreciprocal optical devices such as optical isolators and circulators still present a hurdle towards full integration on optical chips. Driven mainly by cost efficiency and high performance operation, today's commercial nonreciprocal components are based on Faraday rotation effects [1]. Consequently, these devices are bulky and not compatible with integrated photonics platforms.

Practical on-chip integration of nonreciprocal devices demands achieving acceptably large isolation ratios $(\approx -35$ dB$)$ and low insertion losses. In addition, some other features such as polarization independence and large bandwidths are necessary for certain applications.

Recently, there has been intense research activity trying to circumvent some of these difficulties. Given that optical isolators can serve as building blocks for building optical circulators, most of these investigations have focused on integrated optical diodes [2]–[4]. Along these lines, many physical phenomena and optical structures have been proposed to build on-chip optical isolators. These proposals range from using photonic inter-band transitions [5] and nonlinear effects [6] to exploiting nonreciprocal silicon-ring resonators [4], [7]. The interplay between Non-Hermitian optical systems and Kerr nonlinearity has been also proposed as a possible route towards this goal [8]. In addition, optical isolation based on unidirectional optical Bloch oscillations (BO) in waveguide arrays with uniform couplings was also investigated [9]–[11] and modulated waveguide arrays were

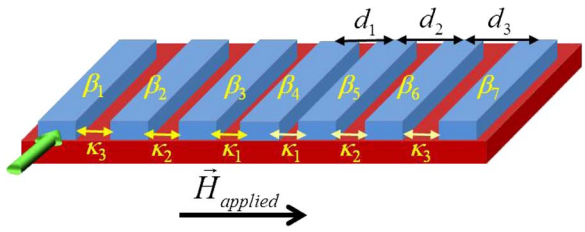


Fig. 1. Schematic depiction of a coupled waveguide array used as optical circulator. The width and/or height of each waveguide elements are carefully designed to introduce a linear ramp in the propagation constant in the backward direction. Nonreciprocal effects are introduced into the structure by depositing magnetic garnet films (not shown here) on top of the array such that a forward propagating optical beam will experience a zero index gradient.

shown to exhibit better performance [12]. In a recent study, a dramatic performance improvement was numerically demonstrated by using an engineered waveguide array with non-uniform coupling coefficients [13].

In the present work, we investigate the operation of the optical structure proposed in [13]. We demonstrate that this device can be used as a multi 4-port optical circulator with large isolation ratios between its ports. In addition, it operates in the linear regime and is compatible with mature silicon-on-insulator (SOI) technologies [9]–[11]. Large bandwidth and efficient coupling to the structure are also among other advantages of the proposed optical structure. Another important and extremely intriguing feature of our proposed design is that it is highly compact. In particular, one can build $N$ such 4-port circulators by using one optical array consisting of $(2N+1)$ waveguide elements. In the following section, we present the proposed optical structure and briefly describe its operation within the context of coupled mode theory. In Section 3, we use beam propagation techniques to systematically investigate the performance of the proposed multi 4-port optical circulator and we show that it has a large bandwidth of operation and can be fabricated within the limits of fabrication tolerances for current technology.

## 2. Coupled Mode Analysis

Fig. 1 depicts a schematic of the optical circulator proposed in this work. Recently, this same geometry was also investigated theoretically for building optical isolators [13]. The structure is made of optical waveguide arrays having coupling coefficients that vary in a square root fashion.

Nonreciprocal effects are introduced to the device by depositing a magnetic film layer (not shown in Fig. 1) on top of the waveguide array [9]–[12]. The design parameters (dimensions of waveguide channels, composition of the magnetic film and the magnitude/direction of the externally applied magnetic field) are tailored such that forward propagating waves experience an unbiased array (where all waveguide elements have the same propagation constant) while backward propagating waves suffer a linear propagation constant ramp of $\delta\beta \neq 0$. Within the context of electromagnetic coupled mode theory, the electric field modal values $E_n(z)$ obey the coupled mode equations [13]–[15]:

$$
\begin{aligned}
i\frac{dE_{-N}}{dz} &= -\delta\beta\ N\ E_{-N} + \kappa\sqrt{2N}E_{-N+1} \\
i\frac{dE_n}{dz} &= \delta\beta\ n\ E_n + \kappa(g_n E_{n-1} + g_{n+1}E_{n+1}), -N < n < N \\
i\frac{dE_N}{dz} &= \delta\beta\ N\ E_N + \kappa\sqrt{2N}E_{N-1}.
\end{aligned} \tag{1}
$$

Here, $g_n = \sqrt{(N+n)(N-n+1)}$ and the coupling coefficients are determined by the parameter $\kappa$. The waveguide array described by Eq. (1) is made of $2N+1$ elements, numbered according to $-N \leq n \leq N$.

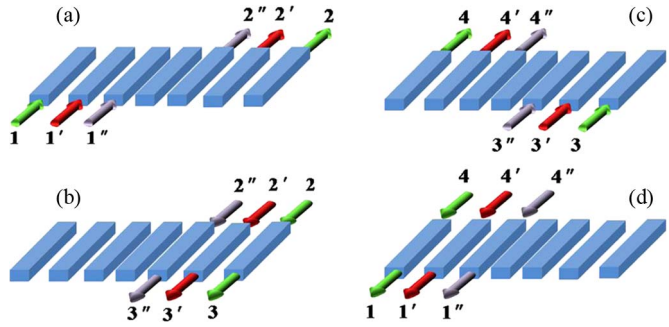


Fig. 2. Illustrates the operation of the waveguide based multi 4-port optical circulator proposed in this work. For an array made of 7 waveguide elements, the device can function as 3 different circulators. Each subplot presents one cycle of the operation mode and the 3 distinct circulators are labeled as (1, 2, 3, 4), $(1', 2', 3', 4')$, and $(1'', 2'', 3'', 4'')$.

It is important to note that Eq. (1) is sufficient to describe both the forward $(\delta\beta = 0)$ and backward $(\delta\beta \neq 0)$ propagation dynamics.

Equation (1) can be investigated analytically and stationary eigenvectors of the form $E_n(z) = A_n \exp(i\lambda_{2N+1,n} z)$ can be obtained in closed form [15]. The particular choice of the function $g_n$ is inspired by Fock space representations of two coupled bosonic modes [13], [15] and leads to an equidistant ladder of eigenvalues:

$$\lambda_{2N+1,n} = n\sqrt{(\delta\beta)^2 + 4\kappa^2}. \tag{2}$$

In Eq. (2), the subscript $2N + 1$ refers to the total number of waveguides and $n$ is the eigenmode index. As described in [13], [15] relation (2) for the eigenvalue spectrum together with the reflection symmetry of the effective optical index around the middle waveguide element lead to perfect state transfer (complete transfer of excitation from one input channel to a different waveguide element at the output) in the forward propagation direction when $\delta\beta = 0$ [13], [15]. In the backward direction, a nonzero $\delta\beta$ leads to surface revivals (the spread and refocusing of an input beam launched at the edge of the array) [13], [15]. In our proposed device, the nonzero backward $\delta\beta$ is chosen to ensure that the revival length in the backward propagation direction matches the complete transfer length of forward propagating excitations (see Section 3 for details on the parameter choice).

Fig. 2 illustrates the conceptual operation of such device for an array made of 7 waveguide elements. For clarity, only the waveguides are depicted without the substrate or the magnetic film layers. In each figure, the arrows point in the propagation direction and arrows of similar color indicate 100% coupling between their corresponding input and output channels. For instance, the green arrow in Fig. 2(a) indicates that during forward propagation, an input beam at port 1 will fully couple to port 2 at the output.

Note that this specific structure can function as three 4-port circulators. These circulators are indicated in Fig. 2 by using primed numbers for labeling the ports. More specifically, the three indicated circulators are labeled by (1, 2, 3, 4), $(1', 2', 3', 4')$, and $(1'', 2'', 3'', 4'')$. The input/output relations of the circulator for the full cycle are presented in Fig. 1(a)–(d). Evidently, for any general array made of $2N + 1$ waveguides, the structure will incorporate $N$ independent circulators.

## 3. Design and Numerical Results

Here, we discuss the realization of the proposed optical circulator in silicon-on-insulator platforms. In particular, we consider an array of ridge waveguides having a gradient in the magneto-optic gyrotropy parameter. As we have mentioned earlier, introducing a transversely magnetized garnet film on top of the waveguide array leads to nonreciprocal propagation dynamics.

Our model structure, shown in Fig. 3, consists of silicon ridges on insulator with a gyrotropic layer deposited on top of each ridge.


Fig. 3. Schematic depiction of Si ridge array cross section with gyrotropy ramp in cover layers.

The complex structure of the iron garnet cover layer allows us to tailor the off-diagonal components (responsible for the gyrotropy) of its dielectric permittivity matrix:

$$\hat{\varepsilon} = \begin{pmatrix} \varepsilon & 0 & ig \\ 0 & \varepsilon & 0 \\ -ig & 0 & \varepsilon \end{pmatrix}. \tag{3}$$

Moreover, the garnet cover layer is engineered to exhibit a gyrotropy parameter $g$ that varies in a stepwise manner from waveguide channel to the next, thus leading to a gradient in the nonreciprocal response across the array. This approach for detuning the waveguides has the advantage of simplifying the fabrication process for silicon arrays as compared to previous proposals where variations in waveguide thickness across the array were employed to produce a nonreciprocal gradient of the propagation constants [9]–[11], [13].

In order to implement the proposed variation in the gyrotropy parameter $g$, we note that garnets have three cation sublattices that can accommodate a wide variety of elements and therefore a wide spectrum of optical properties. These three sublattices have dodecahedral, octahedral, and tetrahedral coordination to the oxygen ions in the garnet, respectively. By tailoring the composition of the dodecahedral site across the structure through varying the substitution level x in $Ce_xY_{3-x}Fe_5O_{12}$, or $Bi_xY_{3-x}Fe_5O_{12}$, a gradient in the magneto-optic properties can be introduced. This control over the substitution-level allows for a control of the gyrotropy parameter and, in turn, will produce a systematic difference in the propagation constants for forward and backward traveling light due to the nonreciprocal phase shift effect.

Admittedly the model we describe here introduces the complication of a composition gradient in the cover layer, a feature yet to be developed for magnetic garnets. This approach calls for combinatorial materials synthesis, successfully employed in other materials systems such as yttrium barium copper oxides but not yet explored for magnetic garnets [16].

The nonreciprocal phase shift effect is used to produce a cancellation of the propagation constant difference $(\delta\beta^f = 0)$ between adjacent channels of the array in the forward direction. This gives rise to mirror symmetry in coupling-constant configuration around the middle waveguide element that together with the equidistant ladder distribution in the eigenvalue spectrum of the system leads to perfect state transfer (complete transfer of excitation from one input channel to its mirror symmetric waveguide element at the output). On the other hand, introducing a nonzero $\delta\beta^b$ in the opposite propagation direction through the nonreciprocal effect $\Delta\beta_n^{nr} = \beta_n^f - \beta_n^b$ (here $\beta_n^f$ and $\beta_n^b$ are the forward and backward propagation constants of the waveguide $n$) breaks the mirror symmetry around the middle channel while preserving the constant eigenvalue gradient, thus leading to surface revivals (the spread and refocusing of an input beam launched at the edge of the array) effects.

The parameter $\delta\beta$ is different for forward and backward propagating waves, $\delta\beta^f \neq \delta\beta^b$ as already discussed. Moreover, for any two adjacent waveguides, labeled $i$ and $i+1$,

$$\delta\beta^f - \delta\beta^b = \left(\beta_{i+1}^f - \beta_i^f\right) - \left(\beta_{i+1}^b - \beta_i^b\right) = \left(\beta_{i+1}^f - \beta_{i+1}^b\right) - \left(\beta_i^f - \beta_i^b\right) = \Delta\beta_{i+1}^{nr} - \Delta\beta_i^{nr} = \delta(\Delta\beta^{nr}). \tag{4}$$

In other words, the difference in propagation constant ramp between forward and backward waves is equal to the ramp in nonreciprocal phase shift per unit length between adjacent waveguides. Under the condition of linear ramp of $\delta\beta$ (including the zero gradient case), the system is described by Eq. (1) and the equidistant ladder distribution of the propagation eingenvalues of the array is given by Eq. (2).

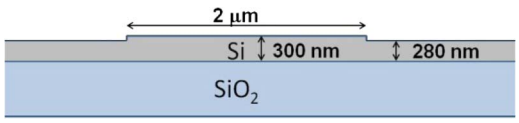


Fig. 4. Design dimensions of silicon ridge waveguides.

TABLE 1

Center to center separations between ridge waveguides in the array (see Fig. 1), corresponding coupling parameters $\kappa_1, \kappa_2, \kappa_3$. Two different inter-waveguide propagation constant steps $\delta\beta^b$ were tested in this study, as shown in the table

| $d_1$ | $d_2$ | $d_3$ | $\delta\beta^b$ (Case 1) | $\delta\beta^b$ (Case 2) |
|---|---|---|---|---|
| 3.68 $\mu m$ | 3.73 $\mu m$ | 3.81 $\mu m$ | 677 $m^{-1}$ | 1350 $m^{-1}$ |
| Coupling $\kappa_1$ | Coupling $\kappa_2$ | Coupling $\kappa_3$ | | |
| 623 $m^{-1}$ | 550 $m^{-1}$ | 462 $m^{-1}$ | | |

In order to investigate the performance of such an array, we assume nonreciprocal ramp values achievable by varying the level of cerium-substitution in a $Ce_xY_{3-x}Fe_5O_{12}$ from x = 1 to x = 0 for ~200 nm- to 300 nm-thick silicon waveguide cores on silicon dioxide slabs at a 1550 nm wavelength [7], [17]. We have also considered steeper gyrotropy gradients such as might be attainable for higher levels of cerium substitution $(x > 1)$ or by combining negative and positive gyrotropy garnets on the cover layer. Steeper gyrotropy gradients yield shorter devices and hence smaller footprints.

The modeling is carried out by designing the array so that $\delta\beta^f = 0$ for forward propagation, and by adjusting the propagation constant ramp in the backward direction to equal the ramp in nonreciprocal phase shift per unit length, $\delta\beta^b = -\delta(\Delta\beta^{nr})$, in accordance with (4). The dependence of the nonreciprocal phase-shift on the gyrotropy parameter $g$ (perturbation theory) is given by

$$\Delta\beta^{nr} = \frac{2\mathrm{Re}\iint dx\,dy(\partial_x H_y)H_y^*(ig/\varepsilon^2)}{\iint dx\,dy|H_y|^2\varepsilon^{-1}}.$$

Here, $H_y$ is the horizontal magnetic-field component of the guided electro-magnetic wave (TM-polarized light) [18]. The integration extends over core, cover and substrate layers of the waveguide. For $Ce_xY_{3-x}Fe_5O_{12}$, and x = 1, the magnitude of $g$ is 0.0024 (polycrystalline garnet film), 0.0063 (epitaxial garnet film) and $\varepsilon = 4.8$ [7]. $g$ varies approximately linearly with substitution level x [19].

Our design consists of 2 $\mu$m-wide, 300 nm-thick silicon ridges with 280 nm-thick slabs, as shown in Fig. 4. These waveguides operate at a 1550 nm wavelength. It is important to note that the relatively wide and shallow waveguide design yield ridge-width fabrication tolerances of ~20 nm for optical surface revivals. Moreover, they avoid the reduction in nonreciprocal performance predicted for narrower silicon ridges [17]. In addition, they exhibit smaller sidewall-roughness-scattering effects compared to high aspect ratio ridge cores [20], thus leading to smaller losses.

Center to center ridge separations are designed to produce coupling constants variations according to Eq. (1) with $\kappa \sim 180$ $m^{-1}$. These separations and the corresponding coupling constants have been tested by semi-vectorial three-dimensional beam-propagation simulations for transverse-magnetic (TM) modes and are listed in Table 1. The $\delta\beta^b$ is modeled by adjusting the design material index for the silicon core in order to yield the desired change in the corresponding mode index of adjacent ridges. The values of the corresponding $\delta\beta^b$ in these simulations are also listed in Table 1.

Owing to the linearity of the system and the symmetry of the structure, we focus our numerical analysis on waveguides 1 and 7. However, all our conclusions here apply equally well to other ports

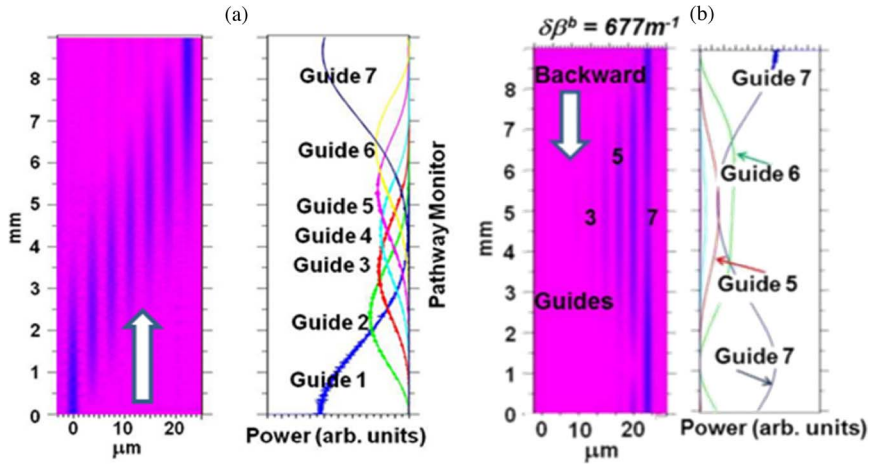


Fig. 5. (a) Forward power transfer for an input beam lunched in waveguide channel 1 when $\delta\beta^f = 0$. (b) Backward propagation showing revival in waveguide 7. Numerical analysis is carried out using semi-vectorial beam-propagation simulation (top view).

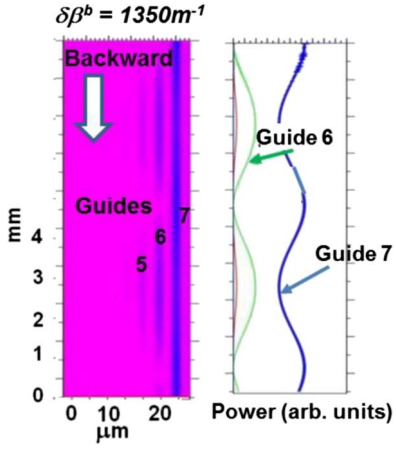


Fig. 6. Backward propagation when $\delta\beta^b = 1350\ \mathrm{m}^{-1}$, showing revivals in waveguide 7, semi-vectorial beam-propagation simulation (top view).

of the 3 different circulators described in Fig. 2. Power transfer efficiency for forward propagation and isolation ratios in the backward direction are computed by monitoring the output power in the beam propagation simulations. Forward transfer efficiency is defined as the ratio of the output power in waveguide 7 to the input power in waveguide 1, excluding coupling losses as well as material absorption. Fig. 5(a) shows the result for forward propagation. More than 95% of the input power in waveguide 1 is transferred to the output waveguide channel 7 in the forward direction. On the other hand, the isolation ratio (computed for backward travelling waves by numerically evaluating the ratio of the output power in waveguide 1 to that of a backward travelling beam launched into waveguide 7) is found to be $-63$ dB for a device length of $\sim$8 mm. This ratio excludes coupling losses. Backward propagation is depicted in Fig. 5(b).

We note that the forward propagation distance needed for complete power transfer can be engineered by controlling the coupling coefficients. For instance doubling $\kappa$ will result in complete transfer after nearly $\sim$4 mm of propagation. This can lead to smaller footprint provided that we also engineer the backward index gradient such that the revival period matches this same propagation distance. As shown in Fig. 6 for a backward propagating beam this can be accomplished by

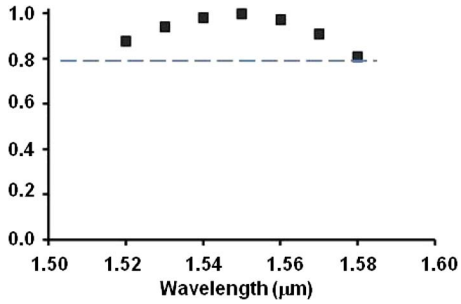


Fig. 7. Forward transmitted power into waveguide 7 as a function of wavelength, normalized to input power.

choosing $\delta\beta^b = 1350\ \text{m}^{-1}$ (see Table 1). Here, also the simulations are carried out using the beam-propagation method.

An important advantage of using waveguide arrays is their relatively wide bandwidth of operation. This feature is confirmed by systematically computing the forward transmission and backward isolations using input optical beams having different wavelengths and launched into the exact same array (designed to operate at 1550 nm wavelength). As shown in Fig. 7, a 50 nm bandwidth for less than 1 dB forward loss is obtained for the simulations. In addition, isolation ratios of better than $-40$ dB and $-35$ dB over 50 nm bandwidths, with peak isolation ratios of $-63$ dB and $-52$ dB at 1550 nm are found for $\delta\beta^b = 677\ \text{m}^{-1}$ and $\delta\beta^b = 1350\ \text{m}^{-1}$, respectively.

## 4. Conclusion

We propose a new optical circulator device based on waveguide arrays engineered to mimic the Fock space representation of a non-interacting two-site Bose–Hubbard Hamiltonian. Coupling constants are adjusted to produce perfect signal transfer between input and output channels in the forward direction. Nonreciprocity is introduced through a gyrotropy gradient in transversely magnetized magnetic garnet cover layers. This results in optical revivals in the backward direction. Numerical simulations yield isolation ratios better than $-40$ dB and as high as $-63$ dB at 1550 nm wavelength. Large bandwidths of operation of 50 nm are also obtained.

## References

[1] B. A. E. Saleh and M. C. Teich, *Fundamentals of Photonics*. Hoboken, NJ, USA: Wiley, 1991.
[2] M. Levy, R. M. Osgood, Jr., H. Hegde, F. J. Cadieu, R. Wolfe, and V. J. Fratello, "Integrated optical isolators with sputter-deposited thin-film magnets," *IEEE Photon. Technol. Lett.*, vol. 8, no. 7, pp. 903–905, Jul. 1996.
[3] J. Fujita, M. Levy, R. M. Osgood, Jr., L. Wilkens, and H. Dötsch, "Waveguide optical isolator based on Mach–Zehnder interferometer," *Appl. Phys. Lett.*, vol. 76, no. 16, pp. 2158–2160, Apr. 2000.
[4] M.-C. Tien, T. Mizumoto, P. Pintus, H. Kromer, and J. E. Bowers, "Silicon ring isolators with bonded nonreciprocal magneto-optic garnets," *Opt. Exp.*, vol. 19, no. 12, pp. 11 740–11 745, Jun. 2011.
[5] Z. Yu and S. Fan, "Complete optical isolation created by indirect interband photonic transitions," *Nat. Photon.*, vol. 3, no. 2, pp. 91–94, Feb. 2009.
[6] L. Fan, J. Wang, L. T. Varghese, H. Shen, B. Niu, Y. Xuan, A. M. Weiner, and M. Qi, "An all-silicon passive optical diode," *Science*, vol. 335, no. 6067, pp. 447–450, Jan. 2012.
[7] L. Bi, J. Hu, P. Jiang, D. H. Kim, G. F. Dionne, L. C. Kimerling, and C. A. Ross, "On-chip optical isolation in monolithically integrated non-reciprocal optical resonators," *Nat. Photon.*, vol. 5, no. 12, pp. 758–762, Dec. 2011.
[8] H. Ramezani, T. Kottos, R. El-Ganainy, and D. N. Christodoulides, "Unidirectional nonlinear PT-symmetric optical structures," *Phys Rev. A., At. Mol. Opt. Phys.*, vol. 82, no. 4, pp. 043803-1–043803-6, Oct. 2010.
[9] P. Kumar and M. Levy, "On-chip optical isolation via unidirectional Bloch oscillations in a waveguide array," *Opt. Lett.*, vol. 37, no. 18, pp. 3762–3764, Sep. 2012.
[10] P. Kumar and M. Levy, "Unidirectional optical Bloch oscillations in asymmetric waveguide arrays," *Opt. Lett.*, vol. 36, no. 22, pp. 4359–4361, Nov. 2011.
[11] M. Levy and P. Kumar, "Nonreciprocal Bloch oscillations in magneto-optic waveguide arrays," *Opt. Lett.*, vol. 35, no. 18, pp. 3147–3149, Sep. 2010.
[12] R. El-Ganainy, P. Kumar, and M. Levy, "On-chip optical isolation based on nonreciprocal resonant delocalization effects," *Opt. Lett.*, vol. 38, no. 1, pp. 61–63, Jan. 2013.

[13] R. El-Ganainy, A. Eisfeld, M. Levy, and D. N. Christodoulides, "On-chip non-reciprocal optical devices based on quantum inspired photonic lattices," *Appl. Phys. Lett.*, vol. 103, no. 16, pp. 161105-1–161105-3, Oct. 2013.
[14] R. El-Ganainy, D. N. Christodoulides, C. E. Rüter, and D. Kip, "Resonant delocalization and Bloch oscillations in modulated lattices," *Opt. Lett.*, vol. 36, no. 8, pp. 1464–1466, Apr. 2011.
[15] R. El-Ganainy, A. Eisfled, and D. N. Christodoulides, "Nonclassical light in coupled optical systems: Anomalous power distribution, Fock space dynamics and supersymmetry," arXiv:1306.5706.
[16] C. Chen, unpublished.
[17] T. Mizumoto, R. Takei, and Y. Shoji, "Waveguide optical isolators for integrated optics," *IEEE J. Quantum Electron.*, vol. 48, no. 2, pp. 252–260, Feb. 2012.
[18] N. Bahlmann, M. Lohmeyer, O. Zhuromsky, H. Dötsch, and P. Hertel, "Nonreciprocal coupled waveguides for integrated optical isolators and circulators for TM-modes," *Opt. Commun.*, vol. 161, no. 4–6, pp. 330–337, Mar. 1999.
[19] M. Gomi, K. Satoh, and M. Abe, "Giant Faraday rotation of Ce-substituted YIG films epitaxially grown by RF sputtering," *Jpn. J. Appl. Phys.*, vol. 27, no. 8, pp. L1536–L1538, Aug. 1988.
[20] P. Dong, W. Qian, S. Liao, H. Liang, C.-C. Kung, N.-N. Feng, R. Shafiiha, J. Fong, D. Feng, A. K. Krishnamoorthy, and M. Asghari, "Low loss shallow-ridge silicon waveguides," *Opt. Exp.*, vol. 18, no. 14, pp. 14 474–14 479, Jul. 2010.